

Determining Total I-131 Activity within a VoI Using SPECT, a UHE Collimator, OSEM, and a Constant Conversion Factor

^{§1}Kenneth F Koral, *Member IEEE*, ²Anastasia Yendiki, ¹Q Lin, ¹Yuni K Dewaraja, *Member IEEE*, ²Jeffrey A Fessler, *Member IEEE*

¹Department of Radiology, ²Department of Electrical Engineering and Computer Science,
University of Michigan, Ann Arbor, Michigan

Abstract—Accurate determination of activity within a volume of interest is needed during radiopharmaceutical therapies. Single-photon emission computed tomography (SPECT) is employed but requires a method to convert counts to activity. We use a phantom-based conversion; that is, we image an elliptical cylinder containing a sphere that has a known amount of 131-I activity inside. The regularized Space Alternating Generalized Expectation (SAGE) algorithm employing a strip-integral detector-response model was employed for reconstruction in previous patient evaluations. With that algorithm and a high-energy collimator, the estimates for sphere activity varied with changes in 1) the level of uniform background activity in the cylinder, 2) the image resolution due to different values of the radius of rotation, R , and 3) the volume of the sphere. When one used those to convert reconstructed counts within a patient tumor into an activity estimate, the resultant value may have been in error because of patient-phantom mismatch. As a potential remedy, in this paper, we use an Ordered Subsets Expectation Maximization (OSEM) algorithm with a 3D depth-dependent detector-response model and an ultra-high-energy collimator. Results after 100 OSEM iterations and using a maximum counts registration show the estimates for sphere activity: 1) have a dependence on the level of background activity with a slope whose absolute magnitude is typically only 0.37 times that with SAGE, 2) are independent of R , and 3) are independent of sphere volume down to and including a sphere volume of 20 cm^3 . We conclude that using a global-average conversion factor to relate counts to activity and no volume-based correction might be reasonable with OSEM.

For a test of that conclusion, target activity is estimated for an anthropomorphic phantom containing a 100 cm^3 spherical tumor centrally located inferior to the lungs. With OSEM-based quantification, using 1) a global-average conversion factor and 2) no volume-based correction, mean bias in the simulated-tumor activity estimate over 20 realizations is -7.37% (relative standard deviation = 5.93%). With SAGE-based quantification, using 1) the conversion factor corresponding to the experimental estimate of background and 2) volume-based correction, the mean bias is -10.7% (relative standard deviation = 2.37%). The mean bias is smaller in a statistically-significant way and relative standard deviation is not more than a factor of 2.5 bigger with OSEM compared to SAGE. In addition, with OSEM, a patient image apparently shows more-highly-resolved features, and the activity estimates for two tumors are increased by an average of 10%, relative to results with SAGE.

Index Terms—SPECT, I-131, ordered subset expectation maximization, registration, activity quantification, reconstruction, recovery coefficient, camera calibration

I. INTRODUCTION

Activity quantification with SPECT has three main components: 1) the reconstruction algorithm, 2) the volume of interest (VoI), and 3) the conversion factor to convert counts to activity. In fairly early work, Israel et al used a percentage of the voxel with maximum counts to set a count threshold for voxels to be included in the target. In phantoms, they got good results for the activity density using a 43% count threshold, but that was for the case without non-target (alias background) activity [1]. Green et al [2] used the dual-window-scatter-correction method [3] and obtained “accurate” activity estimates for a 59cm^3 target at two locations in an elliptical phantom over a wide range of background activities (b varying from 0 to 0.71). Here b is defined as the ratio of the background activity concentration in the cylindrical phantom over the activity concentration in the target. In contrast, in previous phantom measurements, we observed that the total count for a fixed-size spherical target changed when the level of the background activity changed [4]. Our images were reconstructed by a regularized algorithm (SAGE) without detector response [5, 6] and a fixed-size VoI determined from computed tomography (CT) was employed. To account for the dependence of total count on background level, we used a phantom-based conversion factor that varied with the background level [4, 7]. Others have used a count-threshold percent that varied with the background level to choose the size of their VoI [8, 9].

In addition, SPECT activity estimation for small targets was more complicated than for bigger targets, but was of interest for tumor imaging in lymphoma patients being treated with the I-131-labeled monoclonal antibody tositumomab, formerly called anti-B1 [7, 10]. Using positron emission tomography, Hoffman et al pointed out that there was a failure to achieve accurate quantification for objects with one or two dimensions less than twice the full width at half maximum (FWHM) of the imaging system [11]. Kessler et al suggested the use of phantom-based hot-spot and cold-spot recovery coefficients, RCs, to correct for activity-estimate distortions for small VoI [12]. However, others have pointed out problems with that method [13]. With our previous quantification method, we verified that the estimated activity in a sphere with a volume different than that used to determine the phantom-based conversion factor was in error [14]. Therefore, we applied a correction based on hot-spot recovery coefficients determined for spheres. However, Monte Carlo tests that used a voxel-man phantom showed that the resultant activity for a non-spherical target shape was in error by as much as 35% [15].

In this paper, we investigate the employment of OSEM in order to obtain a conversion factor for I-131 activity that is independent of background level while still using a fixed-size VoI derived from CT. OSEM is an inherently-unregularized algorithm [16], and so does not worsen resolution in order to obtain a smoother image. With the use of a detector-response model, it compensates for system blur [17]. Thus, we expect OSEM with a detector-response model to nullify the effects of background level on target activity. With I-131, the addition of a

detector-response model has been said to yield “drastic improvements in clinical image quality”[18]. However, Lalush and Tsui have stated that the accuracy of results from OSEM cannot be predicted, but must be carefully verified empirically[19]. In this paper, we compare our OSEM results to reconstructions of the same data with SAGE.

Also, in this paper, we choose the number of iterations of the OSEM algorithm so as to obviate the need for a recovery coefficient with smaller-volume targets.

Finally, septal penetration is present with the high-energy collimator employed for I-131 imaging in standard practice, and is a complicating factor. Therefore, in this paper we use an ultra-high-energy collimator that reduces septal penetration in order to improve our chances for accurate quantification. In a related investigation [20], we keep quantification features the same, and do an initial comparison of the results from the high-energy and the ultra-high-energy collimator.

The innovation of this research is the particular combination of quantification features for the specific task of activity estimation of I-131 in targets that may have small sizes. As part of the study design, we intentionally compare the procedure using OSEM with detector response to the SAGE procedure as it was carried out for patient measurements. We know that correlations of radiation absorbed dose with response to therapy did not reach statistically-significant levels with those SAGE patient measurements[10], and are looking for improvement with OSEM. One could look for improvement by variations of the SAGE procedure used previously; these variations were not investigated in this research.

II. METHODS

A. Camera and Collimator

The SPECT camera used for both measurements and simulations was a Marconi Medical Inc. triple-headed Prism 3000 with ultra-high-energy-general-all-purpose (UHE) collimation. The collimators were designed for single-photon imaging of a positron-emitting radionuclide. They had a septal thickness of 3.43mm, a hole width from flat to flat of 5.08mm and a hole length of 77.0mm. For each head of the camera, an image of a standard flood source filled with I-131 was taken with a UHE collimator in place. These images were the basis for the standard Prism 3000 uniformity correction. It was calculated, stored, and then used on-the-fly in all subsequent image acquisitions in the standard way.

B. Counts-to-Activity Calibration Measurements

To calibrate the camera, SPECT images of a 200 cm³, known-I-131-activity sphere situated off center along the long axis in an elliptical phantom containing water (Data Spectrum Corp.) were acquired into a 64x64 matrix using a 120-degree circular-orbit with 6 degrees between projections. The 20 projections from each of the 3 heads were combined to yield 60 projections over 360 degrees. The

sphere contained 14.5 MBq (391 μ Ci) of I-131. (This is an appropriate value since it is about half the average tumor activity that the authors had observed 48hrs after therapy for a tumor size in the range of 160 to 250 cm³. This unpublished observation was for lymphoma patients being treated with the I-131-labeled tositumomab.) Uniform-background-activity level in the water was varied to yield four b values, ranging from 0 to 0.37. Each phantom acquisition was carried out at five values of the radius of rotation, R (19, 21, 23, 24.5 and 26cm). In all, 20 separate SPECT data sets were acquired. (Note that the R values cited throughout this paper were as read off of the Prism 3000 display, that is, to the face of a standard collimator. The UHE collimator has a greater thickness than a standard collimator. Since we used the Prism 3000 value consistently for both experimental SPECT acquisitions and for experimental point-source measurements, a correction wasn't needed there. For the Monte Carlo calculations, the difference between the distance to the face of a standard collimator and to the detector crystal when employing the UHE collimator was taken into account.)

C. Modeling Detector Response

To determine FWHM parameters for the OSEM reconstruction, we used experimental point-source measurements at five distances, acquired into a 512x512 matrix. The average behavior of the point source response was modeled by a rotationally-symmetric Gaussian. Width and center location of the Gaussian were determined by non-linear least-squares fitting. Due to the relative simplicity of the function, the peaks and valleys of the hole pattern (see Figure 1) were not tracked; a mean count level was used. The detector response was also assumed to be shift invariant on a plane parallel to the detector; that is, hole pattern changes with sub-pixel shifts of the point source were ignored.

D. Recovery Coefficients

Monte-Carlo simulation was used to generate SPECT projection data that were reconstructed to produce recovery coefficients for spherical volumes different than 200 cm³. A matrix size of 64x64, and three different values of uniform background (b = 0, 0.2 and 0.4) were investigated. The radius of rotation, R, was fixed at 26 cm. Sixty angles over 360 degrees were again employed

E. Reconstruction, Convergence, and Activity Quantification

Reconstruction was carried out with 1) SAGE, and 2) an OSEM algorithm driven by a three dimensional (3D) matrix, each slice of which was associated with a depth and contained a 2D point-source detector response. This OSEM algorithm is more practical (less computing time and memory) than an unregularized SAGE with a full detector-response model would have been. For the OSEM algorithm, the 60 projections were grouped into six subsets. The SPECT system model employed in the OSEM reconstructions projects a 3D volume with attenuation as described by Zeng and Gullberg [17]. Regions outside the 3D volume being

reconstructed are accessed by the detector response model when voxels near the edge are updated. This access is handled by assuming zero values outside the 3D volume in the transverse directions and by repetition of the end slices in the axial direction. Inactive detector elements (those that have zero counts in all projection views) were disregarded in the reconstruction. The initial guess was a filtered back projection image that had been smoothed using a Gaussian with a FWHM of 2.2 cm. All non-positive values of the initial guess were initially set to a very small, positive value to allow for them to be updated.

Convergence was determined on the basis of total counts within the VoI for the target sphere.

In all cases of activity quantification, 1) the attenuation map was derived from energy extrapolation of a registered CT image [21], and 2) scatter compensation was carried out during reconstruction by using a voxel-by-voxel scatter estimate from a triple-energy-window technique [22]. By virtue of the CT-to-SPECT registration, sphere outlines determined for the CT image were used as VoI for the summation of SPECT counts.

F. CT-to-SPECT Registration and VoI Determination

For the SPECT scanning, radioactive markers were placed at 7 ink-marked locations that had been distributed over the elliptical-phantom's curvilinear edge. A CT image of the phantom was also acquired with the radioactive markers replaced by lead beads. The CT image was obtained in a separate imaging session using a General Electric HiSpeed CT/i scanner employing 1cm thick slices. Then, the location of the markers was determined visually in each image set, and the initial transformation for the registration of the CT and SPECT image sets was calculated by least squares minimization of the differences in the paired marker positions employing a rigid-body (rotate-translate) transformation. Scale had been predetermined in each space by a calibration. For the calibration phantom with SAGE reconstruction, this transformation was final. It is the same procedure that was employed for a previous camera calibration with a high-energy collimator[4] and for processing patient data[10].

A refinement to the method for locating the sphere VoI in the SPECT image was used for the calibration-phantom data reconstructed by OSEM with 3D detector response because sphere counts was likely to be more sensitive to registration error with OSEM than with SAGE due to OSEM's higher resolution. The algorithm we employed started with the registration based on the markers and varied translation and rotation so as to maximize the counts in the sphere volume of interest [23]. The size of the VoI relative to the SPECT image was constant. The rationale for the use of this procedure is that, since the background activity surrounding the sphere is uniform, and its concentration is always less than the concentration in the sphere, the registration that maximizes counts for the constant-sized sphere volume of interest is likely to have minimum error. It thus potentially improves on the marker-based registration since that registration requires accurate placement of markers over ink marks, and recognition of the location of the marker centroid in the image. The refinement always produced visually reasonable superimposition of the sphere VoI on the SPECT image and increased the sphere counts by up to 10% for some calibration points. Note that

this refinement only affected the placement of the VoI; no change in the attenuation map was made and no repeat OSEM reconstruction was carried out. Also note that other, simpler methods could be used to improve the accuracy of the CT-to-SPECT registration. Greater attention to the accurate placement of both the radioactive and the highly-attenuating markers in the same location would help the accuracy, as would calculating the centroid of the radioactive distribution for each marker to subpixel precision and input of that centroid into the registration program.

For reconstructions of Monte-Carlo data, the attenuation map and the location and extent of a sphere are known from the input parameters for the simulation. Therefore, no image registration is needed.

For reconstructions of real data, a spherical VoI was determined by 1) visually locating a circle upon the CT image of the central slice through the sphere. 2) visually locating the centers of other circles on adjacent slices and choosing their radius from the number of voxels within the central-slice circle, and from geometrical considerations based on the size of the sphere and the slice thickness. For the patient, tumor outlines were determined on the CT by a radiologist. For all real data, the VoI from CT was transferred to SPECT on the basis of the final registration.

G. Phantom Test

We carried out a test of the bias and variance of the quantification scheme based on OSEM relative to that based on SAGE. A constant registration was applied to each of 20 realizations. This constant registration was specific to the quantification scheme (OSEM-based or SAGE-based). We did not test the absolute bias and variance of either method; such a test would use a separate registration for each realization, since registration error affects the mean bias and the variance. For example, one would expect a higher variance when registration error was included. For the test carried out, we imaged a 100cm³ sphere that contained 28.9 MBq (780 μ Ci) of I-131 and was centrally located in the same elliptical cylinder as that used in the calibration, but with lung and backbone inserted. As indicated above, the imaging was sequentially carried out 20 times. An R value of 21cm was employed. No radioactivity was placed in the lung compartment, or in the tissue-background compartment. This $b = 0$ case is approached clinically when background activity is low. The phantom was a stringent test for both quantification methods because the attenuation and scatter are different than for the calibration phantom due to the presence of the lungs and backbone. Additionally, for the OSEM-based quantification, the global-average CF came from the full range of measured b values (0 to 0.37), while this case was at the minimum of that range ($b=0$).

The test phantom projection data were reconstructed by SAGE or OSEM and the resultant images processed in the same way that the calibration phantom projection data were reconstructed by that particular algorithm and then processed; the rationale was that the procedure for the activity measurement should match that for the calibration. With each algorithm, the 20 image sets were summed to provide the image from which registration parameters were

chosen. Then, as stated above, the same method-specific registration was used for each realization.

For final quantification with SAGE reconstruction: 1) The b value was calculated from the counts and number of voxels in the target and in the non-target part of the phantom. On the basis of this b value, the appropriate CF was determined from the measured calibration curves for CF versus b . 2) From the CF value, an initial activity estimate was calculated. 3) A recovery-coefficient-based correction value was determined for the known volume of the target from the measured calibration curves for RC versus volume. The correction value multiplied the initial activity estimate to produce the final estimate. For the OSEM reconstruction, the global-average CF value from the measured CF-versus- b calibration curves was employed, and no recovery-coefficient correction was used.

Results were evaluated in terms of *bias* defined as:

$$bias = \frac{A_{est} - A_{true}}{A_{true}} * 100\%$$

where A_{est} is the estimated activity, and A_{true} is the known true activity. The mean bias and the relative standard deviation in the bias were computed using standard definitions for those statistics. A test of the statistical significance of the difference in the mean bias from the two quantification methods was carried out using the paired two-sample student t test (Microsoft Excel software).

H. Patient

A previously-untreated lymphoma patient (ID# 76) was imaged with SPECT with $R=24.6\text{cm}$ at 44 hours after a therapy administration of 4.04 GBq (109 mCi) of ^{131}I tositumomab. A CT image employing 1cm -thick slices was also acquired. Since the background for the patient was not uniform, the count maximization approach did not produce a visually-reasonable registration, and so it wasn't used for the OSEM-based quantification even though count maximization had been used for OSEM with the calibration phantom and with the test phantom. For the patient, a more conservative approach was employed for registration. That is, three anatomical control points (simulating internally-placed markers) were chosen for each image set and a rotate-translate registration minimizing the least-square difference between their locations was employed. This registration successfully superimposed the large tumor and the major organs from CT onto SPECT.

Also, the same registration was used for both SAGE-based and OSEM-based quantification of VoI counts. Recall that, in contrast, the registration procedure was different for OSEM compared to that for SAGE for both the calibration phantom and also for the test phantom. Final activity quantification was otherwise as for the test phantom. The volume of each of the two tumors was not known, and so was calculated from the patient CT scan.

III. RESULTS

A. Point Spread Functions

One of the measured point-spread-function images is shown in Figure 1. The distance from the collimator face was 24.5 cm. The hole pattern was quite pronounced due to the thick septa of the ultra-high-energy collimator but the count level never dropped to zero within the response disk. The least-squares fit with a rotationally-symmetric two-dimensional Gaussian went midway between the peaks and valleys of the hole pattern.

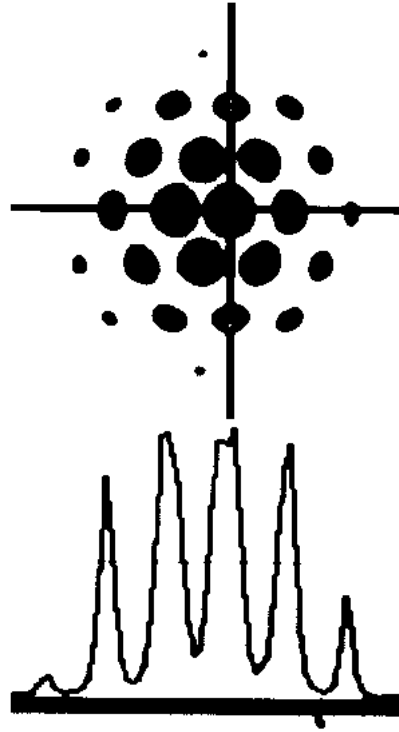


Fig. 1. Projection image from a point source at 24.5 cm in front of the collimator face shows the UHEGAP-collimator hole pattern. For the image at the top, the count required for black has been reduced so as to show more of the hole pattern. Plot at bottom is for the count profile at the location shown in the image by the horizontal line. Here a true linear scale is employed for the count level. Profile corresponding to the vertical line is not shown for simplicity.

B. Convergence

Twenty iterations was sufficient for convergence with SAGE. With OSEM, the convergence pattern for the 200cm^3 sphere using experimental data was found to be very similar with all background levels. Figure 2 shows that pattern. It is seen that convergence was very rapid and the total sphere counts varied little from 20 through 100 iterations. Relative units are sufficient since only the pattern of increase is of interest. They are employed in Figure 2 and 3 because sphere-count values from experiment and simulation cannot be compared since the sphere activity was not the same and the simulated camera sensitivity may not be identical to that for the experimental camera.

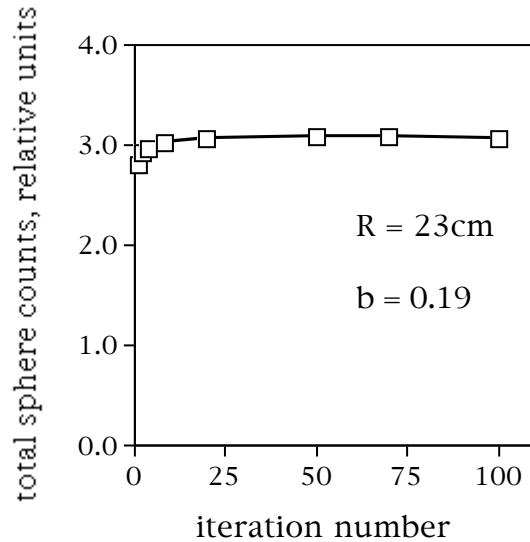


Fig. 2. Total sphere counts versus iteration number with OSEM using experimental data for a 200cm³ sphere.

Convergence for the 200cm³ sphere with zero background using the Monte-Carlo data was also similar. This is shown by the squares in Figure 3B. (Note that even when results were examined after every iteration, no cycling through solutions was seen.) The convergence for the 200cm³ sphere with non-zero background was slower using the Monte-Carlo data. This is shown by the diamonds in Figure 3B. The convergence for smaller spheres with zero background using Monte-Carlo data was again rapid. An example is shown by the squares in Figure 3A. The convergence for smaller spheres with non-zero background using Monte-Carlo data was again slower. An example is shown by the diamonds in Figure 3A.

Because most reconstructions had completely converged after 100 iterations, and because 100 iterations was found to provide good results for the recovery coefficients, (as is shown in Figure 5 and 6 below) 100 iterations was used as the stopping point for all OSEM reconstructions even though 20 was sufficient in some cases.

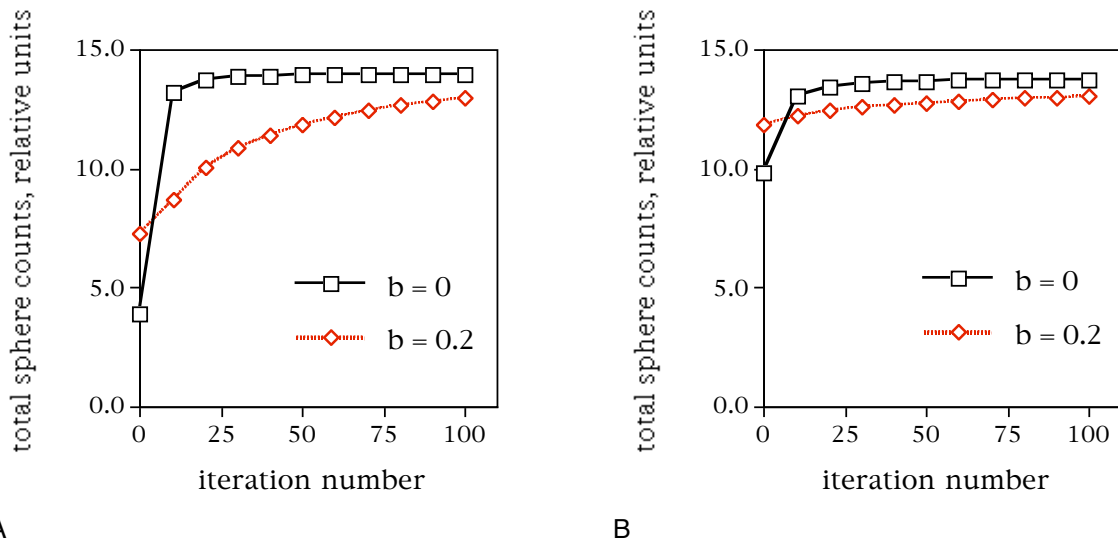


Fig. 3. Total sphere counts versus iteration number with OSEM for Monte-Carlo simulation. Sphere activity is the same for all plots. A) Sphere size=20cm³. B) Sphere size=200cm³.

C. Conversion Factor from Experimental Data

With SAGE reconstruction, CF exhibited a linear dependence on measured b for each of the 5 values of R . A sample dependence is shown by the bottom curve of Figure 4. The units of CF are $(\mu\text{Ci s})^{-1}$. The time in seconds is that of the entire acquisition, that is, the acquisition time of one projection multiplied by the number of projections. The slope had a positive value of $0.310 (\mu\text{Ci s})^{-1}$ because counts within the sphere increased due to the tails of the increasing background. The CF values were also plotted versus R , keeping b constant. Although not shown, these plots all had a linear decrease of CF with R due to worsening resolution as the radius of rotation increased. That is, since the activity concentration of the sphere was greater than that of the background, the counts within the constant-sized-sphere VoI went down as the resolution worsened.

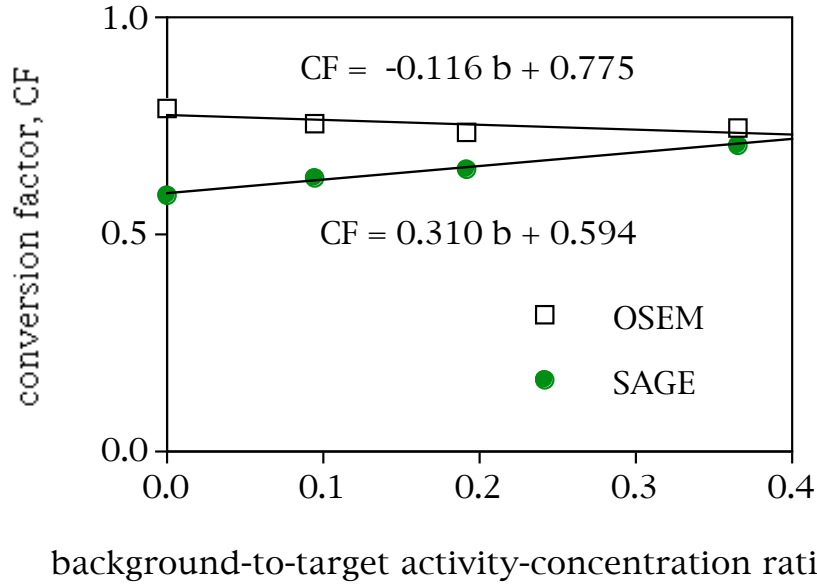


Fig. 4. Counts-to-activity conversion factor, CF, plotted against background-to-target activity-concentration ratio, b. SPECT radius of rotation, R, equaled 23cm.

With OSEM, the linear fit for CF had a larger intercept, $0.775 (\mu\text{Ci s})^{-1}$, than with SAGE, $0.594 (\mu\text{Ci s})^{-1}$, due to the higher resolution of OSEM with 3D detector response (see top curve of Figure 4). Importantly, CF was less dependent on b with OSEM than with SAGE: the absolute value of the slope with OSEM was only 0.37 times the absolute value of the slope with SAGE. Results were similar for all five R values. These results argued for using a single, global-average CF value for all cases with OSEM.

Less importantly, the CF values plotted versus R, keeping b constant, had little or no dependence on R. These plots aren't shown. The result occurred because the change in resolution with a change in the depth of the source due to a change in R was taken into account by the detector-response model.

D. Recovery Coefficients from Monte-Carlo Data.

Plots of recovery coefficient versus sphere volume for $b = 0.2$ are found in Figure 5. With SAGE, recovery of activity was deficient for volumes less than 200cm^3 , as expected from the results with a high-energy collimator previously discussed. Importantly, with OSEM all activity was recovered; the slope of the best-fit line was very small.

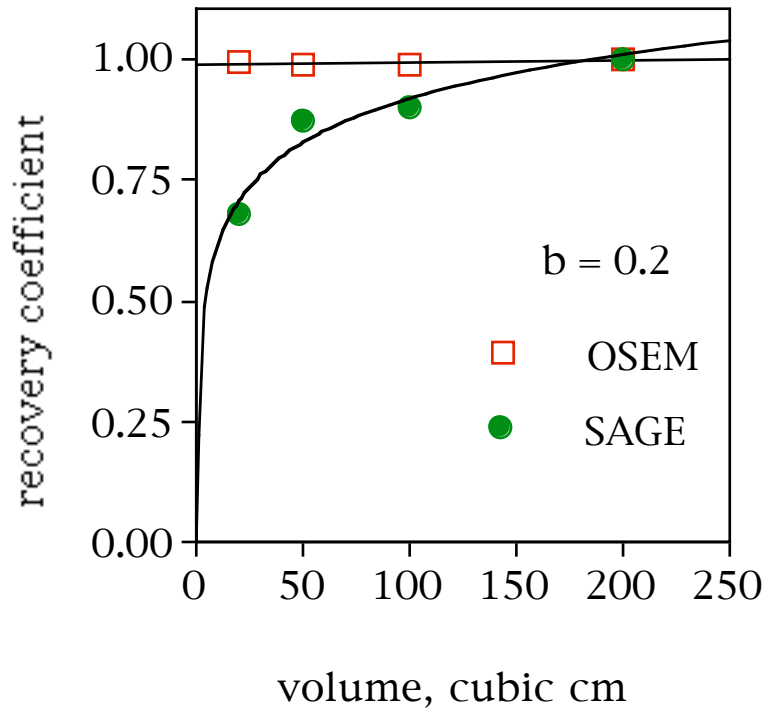


Fig. 5. Recovery coefficient plotted versus sphere volume. Comparison of OSEM result to SAGE result. The background-to-target activity-concentration ratio b is 0.2. The SAGE result is fit with a logarithmic function, the OSEM result with a straight line.

The recovery-coefficient plots with OSEM for all three b values are shown in Figure 6. The data points for $b = 0.2$ are the same as those plotted for OSEM in Figure 5 but without a linear fit. The results can be generally described as a value of 1 independent of volume if one assumes that there is some noise in the data points. This fact indicated that no recovery-coefficient-based correction factor was needed with OSEM employing 3D detector response down to target volumes of 20cm^3 .

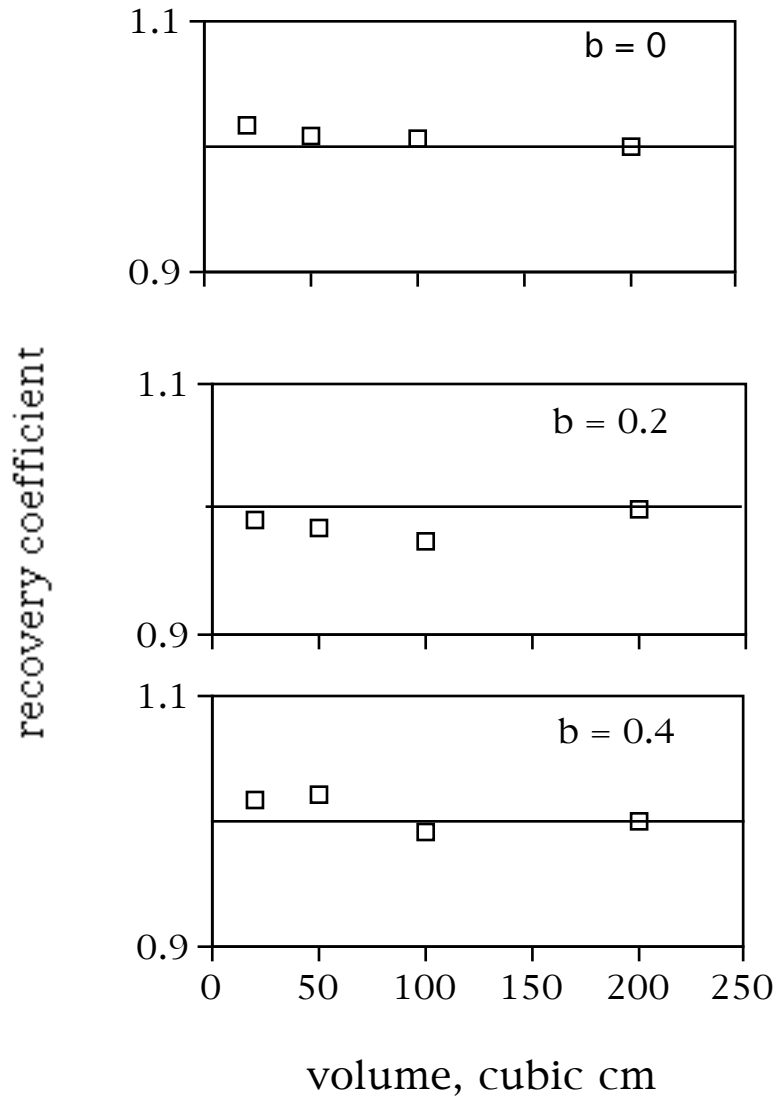


Fig. 6. Plots of RC versus V for three values of the background-to-target activity-concentration ratio, b . Reconstruction is by OSEM. Rather than fits to the data, horizontal lines for the ideal RC value of 1 are shown in each plot.

E. Phantom Test.

With OSEM-based activity quantification, mean bias in the simulated-tumor activity estimate over 20 realizations was -7.37%. The relative standard deviation in the bias value was 5.93%. With SAGE-based activity quantification, the mean bias was -10.7%. The relative standard deviation in the bias was 2.37%. The difference in mean bias was statistically significant. This significance was mainly due to the small variances with both methods, since the difference itself was small. In summary, the mean bias with the OSEM-based quantification was somewhat smaller than with SAGE-based quantification, and the relative standard deviation was not bigger by more than a factor of 2.5.

F. Patient Image Set and Estimates of Tumor Activity

Figure 7 shows a slice that passes through the large tumor for the patient. The tumor outlines were from CT and had been transferred to the SPECT space based on the CT-SPECT registration. The radioiodine distribution for this tumor is seen to be apparently less uniform with the OSEM reconstruction than it had appeared with SAGE reconstruction, due presumably to higher resolution with OSEM and 3D detector response.

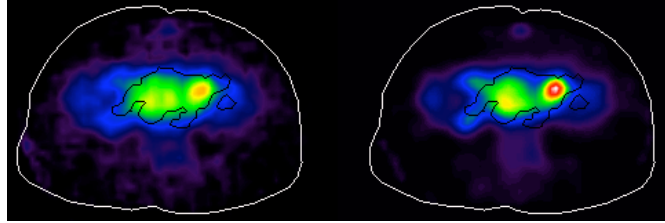


Fig. 7. One slice of the patient image set. Body outline is shown in white. Outline of tumor regions is shown in black. Left: result with SAGE. Right: result with OSEM.

For the same patient, Figure 8 shows two other, more superior slices, which are separated by 8cm. At the bottom of the figure, the apparent kidney-activity concentration with OSEM (right) is larger than the apparent activity concentration with SAGE (left) presumably due to the better resolution with OSEM. At the top, the apparent liver-activity concentration is lower than that in the spleen with both algorithms, but more so with OSEM (right) presumably because the spleen activity does not blur as much into other planes. With OSEM, the apparent blood-activity concentration in the aorta is less than the apparent activity concentration in the spleen (top left); with SAGE these two are equivalent (top right). In other adjacent planes not shown, however, apparent blood concentration is equivalent to apparent spleen concentration with OSEM as well. In general, the blood in the major vessels is better recognized with OSEM presumably due to its better resolution.

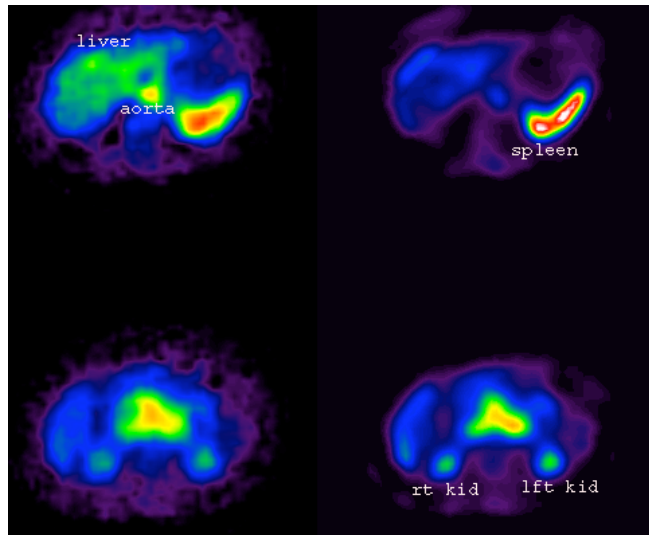


Fig. 8. Two more slices from the patient image set. These are superior to the slice of Figure 7. The tumors no longer appear. Left: result with SAGE. Right: result with OSEM.

The activity estimates for each of the patient's two tumors from OSEM are compared to those from SAGE in Table 1. The activity estimate for both tumors

increased with OSEM; the average increase was 9.8%. Thus, there is initial evidence that the use of OSEM-based quantification has an effect on tumor dosimetry; the effect might lead to improved correlations with response.

TABLE 1. ACTIVITY ESTIMATE FOR TWO PATIENT TUMORS AS A FUNCTION OF QUANTIFICATION METHOD.

| Tumor volume (cubic cm) | Activity in microcuries | | Difference in percent* |
|----------------------------|-------------------------|-------|---------------------------|
| | SAGE | OSEM | |
| 1.6 | 0.311 | 0.336 | 8.11 |
| 1018 | 1248 | 1392 | 11.5 |

$$* \text{ Difference (in percent) } = \{(A_{\text{OSEM}} - A_{\text{SAGE}}) / A_{\text{SAGE}}\} * 100\%$$

IV DISCUSSION AND CONCLUSION

The potential problem with the SAGE-based quantification method is that the calibration phantom (a sphere in a uniform background) is not completely consistent with the physical conditions for a tumor situated within a non-uniform background. Because of the inconsistency, our previous tumor activity measurements for patients [10] may have been inaccurate. That potential inaccuracy motivated us to search for an imaging, reconstruction, and calibration method that would yield an estimate of total target activity independent of the level and distribution of the background activity.

In addition, a problem with employing an RC-based correction is that it is determined using spheres, while it is frequently applied to convoluted tumor shapes. Moreover, since the correction depends on the volume of the target, defining contiguous cancerous lymph nodes as a single tumor, or not, affects the calculated average tumor dose for the patient. Inaccuracy from these two effects can potentially be reduced by the OSEM reconstruction algorithm that employs a 3D detector-response model since our results to date indicate that with that algorithm an RC-based correction isn't needed down to 20cm³. Whether inaccuracy in activity quantification of tumors can actually be reduced will need to be investigated in the future.

The procedure in this paper of obtaining a good fit to the gross shape of the point-source response using a relatively simple function contrasts with one that seeks a function that duplicates the peaks and valleys in the hole pattern. The latter approach has been pursued by another group for a special-purpose collimator and has yielded high-resolution images [24]. However, it has the disadvantage that the point-spread function is not completely shift invariant, which adds to the complexity of the reconstruction.

Since a variety of convergence patterns was encountered with OSEM, factors that might affect convergence were investigated. This investigation was carried out for the 20cm³ sphere. The factors were 1) a different smoothing for the initial filtered backprojection image, instead of the usual 2.2-cm-FWHM smoothing, 2) a different method for defining the VoI (more or less finely sampled at the sphere edge), and 3) a point spread function generated from Monte-Carlo data rather than the one from the experimental data. The different

smoothing tested was with no smoothing, or with a 6.5cm FWHM. No factor had a large effect. It appears that when the case is complicated by background and a smaller sphere size, and the data are statistically noisy, as they were in our Monte Carlo simulation, the convergence is more complicated than for a large sphere with less-noisy data, as they were in the experiments. For a point source, increased background slows down the resolution recovery with an increase in the number of iterations [25]. Since it isn't clear to us that that effect straightforwardly carries over to sphere total counts, it is our opinion that the effect of each of the aforementioned factors (background, size and noise) will need to be checked further in the future.

With the present OSEM method, the invariance of CF with changes in the radius of rotation at a constant b value indicates that OSEM with depth-dependent detector response compensates for the resolution change of the sphere with depth very well. The slight negative slope of the CF versus b plot at a constant radius of rotation indicates a slight dependence of total sphere counts on the distribution of activity within the field of view. One possible explanation is the non-linear nature of iterative algorithms, and their object-dependent spatial-resolution properties. Our depth-dependent resolution measurements would not take account of these properties. In any case, the slight dependence of CF on b can be viewed as not substantial.

Therefore, with OSEM reconstruction, we employed a single, constant conversion-factor value for the test and patient measurements in this paper. The value was the calculated global average of all values from the calibration measurements. These measurements were representative of the expected range of average-background-to-target activity concentration and radius in patient imaging. A benefit of such a global-average conversion factor is ease of implementation.

The OSEM-based activity quantification with a global-average CF and no recovery-coefficient-based correction showed a statistically-significant improvement in accuracy over the SAGE-based method for estimating the total activity in a 100cm^3 sphere located within an anthropomorphic phantom. Further investigation is needed to determine how well the quantification works in estimating activity in a variety of situations.

The patient image set apparently had better resolution using OSEM with 3D detector response compared to that using SAGE. This improved resolution may be useful in improving the accuracy of SPECT-to-CT registration in patients because the resolution of the OSEM reconstruction will more nearly match that of the CT image set. This improved matching may stabilize the computation of the mutual information when it is maximized to establish a registration. It may also help in the visual judgment of the relative quality of different potential registrations.

The estimates for tumor activity for two tumors were increased by an average of 9.8%. Such changes might lead to more accurate tumor dosimetry and improved correlations with response when OSEM-based activity quantification is employed.

V ACKNOWLEDGMENT

Grants R01 CA87955, R01 CA80927, and R01 EB00218 awarded by the National Institutes of Health, United States Department of Health and Human Services and Grant BES9982349 awarded by the National Science Foundation supported this research. The contents of the paper are solely the responsibility of the authors and do not necessarily represent the official views of the funding agencies.

VI REFERENCES

- [1] O. Israel, G. Iosilevsky, D. Front, L. Bettman, A. Frenkel, S. Ish-Shalom, M. Steiner, M. Ben-Harush, and G. M. Kolodny, "SPECT quantitation of iodine-131 concentration in phantoms and human tumors," *J Nucl Med*, vol. 31, pp. 1945-9, 1990.
- [2] A. J. Green, S. E. Dewhurst, R. H. Begent, K. D. Bagshawe, and S. J. Riggs, "Accurate quantification of 131I distribution by gamma camera imaging," *Eur J Nucl Med*, vol. 16, pp. 361-5, 1990.
- [3] R. J. Jaszczak, K. L. Greer, C. E. Floyd, C. C. Harris, and R. E. Coleman, "Improved SPECT Quantification Using Compensation for Scattered Photons," *Journal of Nuclear Medicine*, vol. 25, pp. 893-900, 1984.
- [4] Y. Dewaraja, J. Li, and K. Koral, "Quantitative I-131 SPECT with triple energy window compton scatter correction," *IEEE Transactions On Nuclear Science*, vol. 45, pp. 3109-3114, 1998.
- [5] J. A. Fessler and A. O. Hero, "Space-Alternating Generalized Expectation-Maximization Algorithm," *IEEE Transactions on Signal Processing*, vol. 42, pp. 2664-2677, 1994.
- [6] J. A. Fessler and A. O. Hero, "Penalized Maximum-Likelihood Image-Reconstruction Using Space- Alternating Generalized EM Algorithms," *IEEE Transactions On Image Processing*, vol. 4, pp. 1417-1429, 1995.
- [7] K. F. Koral, Y. Dewaraja, J. Li, C. L. Barrett, D. D. Regan, K. R. Zasadny, S. G. Rommelfanger, I. R. Francis, M. S. Kaminski, and R. L. Wahl, "Initial results for Hybrid SPECT--conjugate-view tumor dosimetry in 131I-anti-B1 antibody therapy of previously untreated patients with lymphoma," *J Nucl Med*, vol. 41, pp. 1579-86., 2000.
- [8] Y. E. Erdi, B. W. Wessels, M. H. Loew, and A. K. Erdi, "Threshold estimation in single photon emission computed tomography and planar imaging for clinical radioimmunotherapy," *Cancer Res*, vol. 55, pp. 5823s-5826s, 1995.
- [9] Y. E. Erdi, O. Mawlawi, S. M. Larson, M. Imbriaco, H. Yeung, R. Finn, and J. L. Humm, "Segmentation of lung lesion volume by adaptive positron emission tomography image thresholding," *Cancer*, vol. 80, pp. 2505-9, 1997.
- [10] K. F. Koral, Y. Dewaraja, J. Li, Q. Lin, D. D. Regan, K. R. Zasadny, S. G. Rommelfanger, I. R. Francis, M. S. Kaminski, and R. L. Wahl, "Update on hybrid conjugate-view SPECT tumor dosimetry and response in 131I-tositumomab therapy of previously untreated lymphoma patients," *J Nucl Med*, vol. 44, pp. 457-64, 2003.
- [11] E. J. Hoffman, S. C. Huang, and M. E. Phelps, "Quantitation in positron emission computed tomography: 1. Effect of object size," *J Comput Assist Tomogr*, vol. 3, pp. 299-308, 1979.
- [12] R. M. Kessler, J. R. Ellis, Jr., and M. Eden, "Analysis of emission tomographic scan data: limitations imposed by resolution and background," *J Comput Assist Tomogr*, vol. 8, pp. 514-22., 1984.

- [13] L. Geworski, B. O. Knoop, M. L. de Cabrejas, W. H. Knapp, and D. L. Munz, "Recovery correction for quantitation in emission tomography: a feasibility study," *Eur J Nucl Med*, vol. 27, pp. 161-9, 2000.
- [14] K. F. Koral and Y. Dewaraja, "I-131 SPECT activity recovery coefficients with implicit or triple-energy-window scatter correction," *Nuclear Instruments & Methods in Physics Research Section A- Accelerators Spectrometers Detectors and Associated Equipment*, vol. 422, pp. 688-692, 1999.
- [15] Y. K. Dewaraja, M. Ljungberg, and K. F. Koral, "Monte Carlo evaluation of object shape effects in iodine-131 SPET tumor activity quantification," *Eur J Nucl Med*, vol. 28, pp. 900-6, 2001.
- [16] H. M. Hudson and R. S. Larkin, "Accelerated Image-Reconstruction Using Ordered Subsets of Projection Data," *IEEE Transactions On Medical Imaging*, vol. 13, pp. 601-609, 1994.
- [17] G. L. Zeng and G. T. Gullberg, "Frequency-Domain Implementation of the 3-Dimensional Geometric Point Response Correction in Spect Imaging," *IEEE Transactions on Nuclear Science*, vol. 39, pp. 1444-1453, 1992.
- [18] B. M. W. Tsui, X. D. Zhao, S. Sayeram, E. C. Frey, S. W. Falen, and W. H. McCartney, "Evaluation of Collimator-Detector Response Compensation in Tumor SPECT using Medium- and High-Energy Collimators," presented at IEEE Medical Imaging Conference, Lyon France, 2000.
- [19] D. S. Lalush and B. M. Tsui, "Performance of ordered-subset reconstruction algorithms under conditions of extreme attenuation and truncation in myocardial SPECT," *J Nucl Med*, vol. 41, pp. 737-44, 2000.
- [20] K. F. Koral, A. Yendiki, Q. Lin, Y. K. Dewaraja, and J. A. Fessler, "Update on HE vs UHE Collimation for Focal Total-activity Quantification in I-131 SPECT," *Conference Proceedings (CD ROM) for IEEE MIC Conference, Portland OR, Oct. 19-25, 2003*.
- [21] K. F. Koral, H. Zaidi, and M. Ljungberg, "Medical imaging techniques for radiation dosimetry," in *Therapeutic applications of Monte Carlo calculations in Nuclear Medicine*, H. Zaidi and G. Sgouros, Eds. Bristol and Philadelphia: Institute of Physics Publishing, 2003, pp. 55-83.
- [22] K. Ogawa, Y. Harata, T. Ichihara, A. Kubo, and S. Hashimoto, "A Practical Method for Position-Dependent Compton-Scatter Correction in Single Photon-Emission CT," *IEEE Transactions on Medical Imaging*, vol. 10, pp. 408-412, 1991.
- [23] J. Li and K. F. Koral, "An algorithm to adjust a rigid CT-to-SPECT fusion so as to maximize tumor counts from CT VoI in 131-I therapies.," presented at IEEE Medical Imaging Conference, San Diego CA, 2001.
- [24] D. E. Gonzalez-Trotter, J. E. Bowsher, and R. J. Jaszczak, "Improved I-131 SPECT resolution through modeling individual medium-energy collimator holes.," presented at IEEE Medical Imaging Conference, Lyon France, 2000.
- [25] T. S. Pan, D. S. Luo, V. Kohli, and M. A. King, "Influence of OSEM, elliptical orbits and background activity on SPECT 3D resolution recovery," *Phys Med Biol*, vol. 42, pp. 2517-29, 1997.